Probe Report

Title: Identification of activators for the M2 isoform of human pyruvate kinase Version 3

Authors: Matthew B. Boxer,[a] Jian-kang Jiang, [a] Matthew G. Vander Heiden,[b,c] Min Shen, [a] Henrike Veith, [a] Lewis C. Cantley,[d,e] Craig J. Thomas [a]

[a)] NIH Chemical Genomics Center, National Human Genome Research Institute, National Institutes of Health, 9800 Medical Center Drive, MSC 3370 Bethesda, Maryland 20850, [b)] Koch Institute at MIT, Cambridge, MA 02139, USA [c)] Dana Farber Cancer Institute, Boston, Massachusetts 02115, [d)] Department of Systems Biology, Harvard Medical School, Boston, Massachusetts 02115, and [e)] Division of Signal Transduction, Beth Israel Deaconess Medical Center, Boston, Massachusetts 02115

Version #3

Submitted 2/24/2011

Assigned Assay Grant #: R03 MH085679

Screening Center Name & PI: NIH Chemical Genomics Center & Dr. Christopher P. Austin

Chemistry Center Name & PI: NIH Chemical Genomics Center & Dr. Christopher P. Austin

Assay Submitter & Institution: Dr. Matthew George Vander Heiden, Harvard

PubChem Summary Bioassay Identifier (AID): 2095

Abstract:

The expression of human pyruvate kinase M2 (hPK-M2) in cancer cells appears to be critical for tumor cell growth and proliferation in vivo. Because the PK-M2 isoform is expressed in all cancer cells studied, it represents a target for drug development that could potentially enable tumor cells to return to a normal state of metabolism. If this novel strategy for targeting malignancy were successful, it would be applicable to diverse types of cancer. The probes ML203, ML202 and ML170 represent 3 preclinical lead series that are highly specific allosteric activators of the tumor-specific isoform of human pyruvate kinase (M2 isoform). Both probes affect the cooperativity of phosphoenolpyruvate (PEP) binding, with little effect on adenosine diphosphate (ADP) binding, in a manner similar to FBP.

Probe Structure & Characteristics:

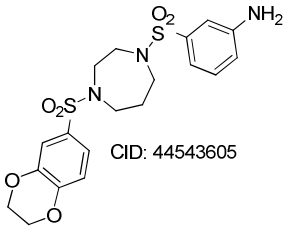

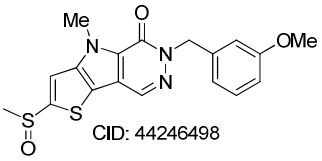

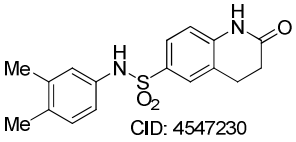

ML203 **ML202** **ML170**

CID/ML#	Target Name	IC_{50}/EC_{50} (nM) [SID, AID]	Anti-target Name(s)	IC_{50}/EC_{50} (µM) [SID, AID]	Fold Selective	Secondary Assay(s) Name: IC_{50}/EC_{50} (nM) [SID, AID]
44543605/ ML203	hPyk-M2	129 [87225694, 2533]	hPyk-M1, -R, and -L	Inactive against all 3 isoforms [87225694, 2536, 2534, 2535]	>100 fold over all 3 isoforms	LDH assay 92 [87225694, 2576]
44246498/ ML202	hPyk-M2	73 [85267884, 2533]	hPyk-M1, -R, and -L	Inactive against all 3 isoforms [85267884, 2536, 2534, 2535]	>100 fold over all 3 isoforms	LDH assay 410 [85267884, 2576]
4547230/ ML170	hPyk-M2	163 [85176568, 1751]	hPyk-M1, -R, and -L	Inactive against all 3 isoforms [85176568, 2536, 2534, 2535]	>100 fold over all 3 isoforms	LDH assay 146 [85176568, 2576]

Recommendations for scientific use of these probes:

The metabolism of cancer cells is altered to support rapid proliferation. Several biological factors have been implicated in the abnormal metabolic state of cancer cells, including the expression of a tumor cell specific pyruvate kinase isozyme (hPyk-M2). Pharmacological activators of hPyk-M2 may be an approach for altering the classic Warburg effect characteristic of aberrant metabolism in cancer cells yielding a novel anti-proliferation strategy. Prior to our discovery of these hPyk-M2 activators, there were no reported small molecule modulators of this enzyme. These compounds can be used to study the metabolic state of cancer cells and as a lead for the development of anti-cancer agents.

1 Introduction

One of the most prominent distinctions between healthy and cancerous tissues is the differing energetic and nutritional needs associated with the rapid proliferative nature of cancer cells. The original observation that cancer cells maintain a different metabolic state relative to non-proliferating cells was made by Otto Warburg in the 1920's, and today, the Warburg effect is a highly studied area of research[1-3]. In normal cells, glucose is primarily metabolized by glycolysis and oxidative phosphorylation when oxygen is available. A key aspect of the Warburg effect is that cancer cells will produce increased amounts of lactate, even in aerobic conditions. Glycolysis is a multistep process that ultimately converts glucose into two equivalents of pyruvate. Further metabolism by oxidative phosphorylation involves the conversion of pyruvate to acetyl-CoA and entry into the Krebs cycle, with the potential of providing additional ATP. In cancer cells, this metabolism is altered and pyruvate is instead converted to lactic acid even under aerobic conditions. The mechanism(s) that drive this altered metabolism in cancer cells are not fully understood. One contributor, however, is the differential expression of two human isozymes of pyruvate kinase (Pyk)[4]. The final step of glycolysis involves the conversion of phosphoenolpyruvate (PEP) and ADP to pyruvate and ATP by Pyk. This process yields one equivalent of ATP per PEP. Tanaka and coworkers were the first to show that alternative pre-mRNA splicing yields the M1 and M2 forms of pyruvate kinase (hPykM1 and hPyk-M2)[5]. hPykM2 is widely expressed in undifferentiated embryonic tissues and, at some point during development, differentiated tissues switch to express hPykM1. A second gene produces two additional Pyk isozymes, based on alternative splicing events, to produce PKL and PKR; these are expressed in specific adult tissues. An important realization in cancer biology was the recognition that all cancer cells revert back to the hPykM2 isozyme. In tumor cells, hPykM2 has been reported to exist primarily in its low activity, dimeric form. Functionally, the down-regulation of hPykM2 activity in cancer cells is thought to aid in shunting key glycolytic intermediates toward pathways where they, in turn, are utilized as precursors for lipid, amino acid and nucleic acid synthesis. Rapidly proliferating cells, such as undifferentiated embryonic tissue and cancer cells, require increased amounts of these fundamental cellular building blocks. Thus, the down-regulation of hPykM2 activity provides a purposeful divergence from catabolic metabolism aimed at energy production, toward an anabolic state aimed at providing the needed resources for rapid cellular construction. Recent work has shown that replacement of hPykM2 with hPykM1 in cancer cells can relieve the Warburg effect and promote

oxidative cellular metabolism characteristic of differentiated cells[6]. Further, an assessment of growth *in vivo* of human lung cancer cells engineered to express only hPykM1 showed delayed tumor formation in nude mouse xenografts. The tumors that did form in this model were shown to have re-expressed hPykM2. In a related study, it was demonstrated that hPykM2 has high affinity for binding phosphotyrosine peptides[7]. Protein tyrosine phosphorylation is increased in tumor cells as a consequence of oncogenic intracellular signaling events that also drive uptake of excess nutrients. Binding of hPykM2 to tyrosine phosphorylated proteins catalyzes the release of FBP from the enzyme, and further down-regulates hPykM2 activity to promote entry of glycolytic intermediates into biosynthetic pathways. Taken as a whole, these data suggest a therapeutic strategy whereby activation of hPykM2 may restore normal cellular metabolism to a state characteristic of normal differentiated cells. The goal of this project was to find pharmacological activators of hPykM2 to test this theory. Three unique chemotypes were discovered as potent hPykM2 activators, and all show similar potencies (<150nM with high efficacy).

2 Materials and Methods

General Methods for Chemistry. All air or moisture sensitive reactions were performed under positive pressure of nitrogen with oven-dried glassware. Anhydrous solvents such as dichloromethane, *N,N*-dimethylforamide (DMF), acetonitrile, methanol and triethylamine were obtained by purchasing from Sigma-Aldrich. Preparative purification was performed on a Waters semi-preparative HPLC. The column used was a Phenomenex Luna C18 (5 micron, 30 x 75 mm) at a flow rate of 45 ml/min. The mobile phase consisted of acetonitrile and water (each containing 0.1% trifluoroacetic acid). A gradient of 10% to 50% acetonitrile over 8 minutes was used during the purification. Fraction collection was triggered by UV detection (220 nM). Analytical analysis was performed on an Agilent LC/MS (Agilent Technologies, Santa Clara, CA).

Method 1: A 7 minute gradient of 4% to 100% Acetonitrile (containing 0.025% trifluoroacetic acid) in water (containing 0.05% trifluoroacetic acid) was used with an 8 minute run time at a flow rate of 1 mL/min. A Phenomenex Luna C18 column (3 micron, 3 x 75 mm) was used at a temperature of 50°C.

Method 2: A 3 minute gradient of 4% to 100% Acetonitrile (containing 0.025% trifluoroacetic acid) in water (containing 0.05% trifluoroacetic acid) was used with a 4.5 minute run time at a flow rate of 1 mL/min. A Phenomenex Gemini Phenyl column (3 micron, 3 x 100 mm) was used at a temperature of 50 °C.

Purity determination was performed using an Agilent Diode Array Detector on both Method 1 and Method 2. Mass determination was performed using an Agilent 6130 mass spectrometer with electrospray ionization in the positive mode. ^{1}H NMR spectra were recorded on Varian 400 MHz spectrometers. Chemical Shifts are reported in ppm with tetramethylsilane (TMS) as internal standard (0 ppm) for $CDCl_3$ solutions or undeuterated solvent (DMSO-h6 at 2.49 ppm) for DMSO-d6 solutions. All of the analogs for assay have purity greater than 95% based on both analytical methods. High resolution mass spectrometry was recorded on Agilent 6210 Time-of-Flight LC/MS system. Confirmation of molecular formula was accomplished using electrospray ionization in the positive mode with the Agilent Masshunter software (version B.02).

2.1 Assays

To develop a robust assay for PK, we took advantage of a well-utilized luminescent assay detection system for protein kinases[8,9]. Typically, these assays use the ATP-dependent reaction catalyzed by firefly luciferase to measure ATP depletion by protein kinases. In the present assay, we applied this assay to

measure ATP production catalyzed by PK. This provides for a robust increase in luminescent signal upon ATP product formation (Figure 1). The primary high-throughput screen was performed in 1536-well microtiter plates using 4µl/well assay volume with final concentrations of 0.1nM human PK M2, 0.5mM PEP, and 0.1mM ADP in assay buffer that contained 50mM Imidazole pH 7.2, 50mM KCl, 7 mM MgCl2, 0.01% Tween, and 0.05% BSA. For compound transfer, we used a pintool equipped with 1536 pins that each transferred 23nl of a DMSO solution containing compound. The enzymatic reaction was allowed to proceed for 60 minutes, and then ATP was detected using a bioluminescent detection reagent containing D-luciferin and firefly luciferase (Kinase-Glo, Promega). The detection reagent also effectively stopped the PK reaction. Luminescence was then measured on the Perkin Elmer Viewlux using an exposure of 2 secs (with 2X binning). The final concentration of DMSO in the enzyme assay is 0.5%, and was found not to affect the assay signal.

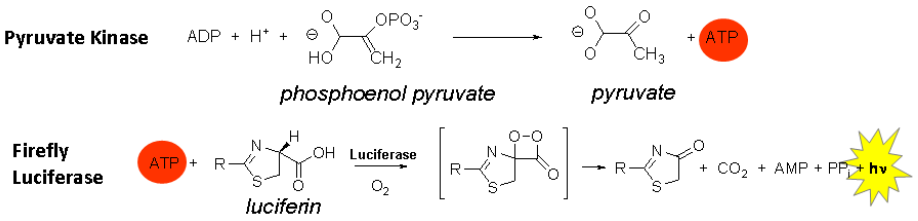

Figure 1. Pyruvate kinase-luciferase coupled assay

All compounds were screened using a qHTS approach, where compounds are assayed using at least seven concentrations to generate concentration-response curves for every compound. The methodology for creating a concentration-titration series between successive copies of library plates for the purpose of large-scale titration-based screening has been described[9]. Briefly, in qHTS, an inter-plate dilution method is used where the first plate contains the highest concentration of a set of compounds in DMSO, while subsequent plates contain the same compounds in the same well locations, but at successive lower concentrations. Using the protocol outlined above, we calculated a plate throughput of 18 plates/hr or approximately 7 samples/sec on the Kalypsys robotic system, which means that a 7 point CRC was obtained every second on the robotic system.

Center summary of the primary screen:

Assay protocol:

Table 1. Final optimized 1536-well assay protocol

Step	Parameter	Value	Description
1	Reagent	3µl	PEP/hPK-M2 buffer (0.5mM and 0.1nM final, respectively)
2	Controls	23nl	Activator control NCGC00031955 (CID_654376)
3	Library compounds	23nl	57 µM to 3.7 nM dilution series
4	Reagent	1µl	ADP buffer (0.1 mM final)
5	Incubation time	1 hr	Room temperature
6	Reagent	2µl	Kinase-Glo
7	Assay readout	Luminescence	ViewLux

Step	Notes
1	Greiner white solid plates; 4 tips dispense to all wells except column 3 of buffer 0.133nM hPK-M2, 0.67mM PEP, 50mM Imidazole pH 7.2, 50mM KCl, 7mM MgCl2, 0.01% Tween, 0.05% BSA. Column 3, 1 tip of same buffer without hPK-M2.
2	Column 1, NCGC00031955 (CID_654376, SID_851783) Activator titration 57µM start, 16 points in duplicate 1:2 dilutions; Column 2 neutral, DMSO only; Column 3 no enzyme; Column 4, top 16 rows are NCGC0031955 (CID_654376, SID_851783) at 57µM, bottom 16 rows are DMSO only.
3	Pintool transfer (tip wash sequence; DMSO, iPA, MeOH, 3-s vacuum dry)
4	ADP in same 4 tips dispense to all wells of buffer containing 0.4mM ADP (final assay 0.1mM), 50mM Imidazole pH 7.2, 50mM KCl, 7mM MgCl2, 0.01% Tween, 0.05% BSA.
5	Plates covered with stainless steel rubber gasket-lined lids containing pin holes for gas exchange.
6	Kinase-Glo detection. Luciferase-based detection of ATP product.
7	Perkin Elmer ViewLux, clear filter luminescent read.

Confirmatory LDH kinetic assay

All compounds were also tested in a kinetic mode by coupling the generation of pyruvate by pyruvate kinase to the depletion of NADH through lactate dehydrogenase. For PKM2, 3µl of substrate mix (final concentration, 50mM Tris-Cl pH 8.0, 200mM KCl, 15mM $MgCl_2$, 0.1mM PEP, 4.0mM ADP, and 0.2mM NADH) was dispensed into Kalypsys black-solid 1,536 well plates using the Aurora Discovery

BioRAPTR Flying Reagent Dispenser (FRD; Beckton-Dickenson, Franklin Lakes, NJ) and 23nl of compounds were delivered via a Kalypsys pin tool; then, 1 µL of enzyme mix (final concentrations, 10nM hPK-M2 and 1µM of LDH) was added. Plates were immediately placed in ViewLux (Perkin Elmer) and NADH fluorescence was determined at 30 second exposure intervals for between 3 and 6 minutes. Data were normalized to the uninhibited and EC_{100} activation using known activators, such as fructose-1,6-bis-phosphate. The data has been deposited in PubChem (AID: 1540 and 2576). Follow-up of synthesized analogs was determined using the same protocol (PubChem AIDs for L, M1 and R bioluminescent assays are 2625, 2620, and 2562).

Anti-target assay(s)

The same assay system was utilized to examine all of the activity of all probes and all related analogs versus the stated anti-targets PKL, PKM1 and PKR (PubChem AIDs for L, M1 and R bioluminescent assays are 2625, 2620, and 2562).

2.2 Probe Chemical Characterizations

Chemotype #1

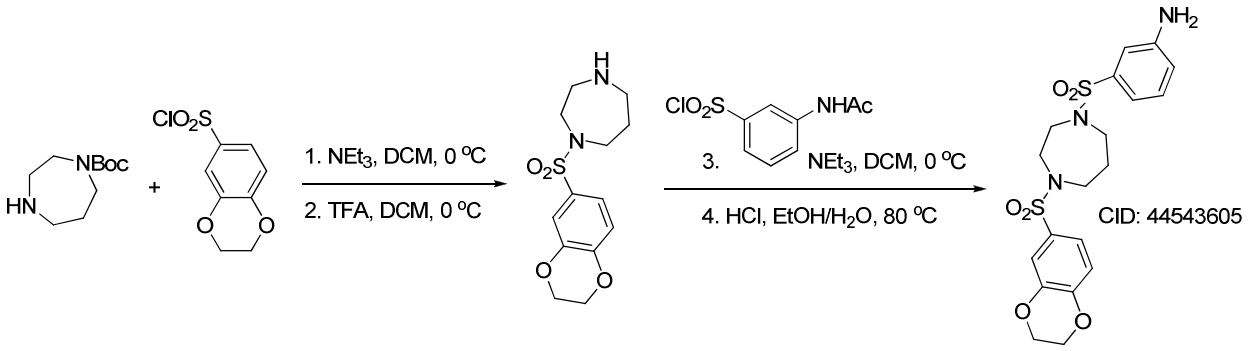

NCGC00185916/SID:87225694/CID:44543605/ML203 ^{1}H NMR (400 MHz, DMSO-d_6) δ ppm 7.18 (m, 3 H), 6.98 - 7.09 (m, 2 H), 6.81 - 6.97 (m, 2 H), 4.18 - 4.36 (m, 4 H), 3.08 - 3.21 (m, 8 H), 1.66 - 1.83 (m, 2 H); LC/MS: Method 1, retention time, 5.017 min; Method 2, retention time 3.704 min; HRMS: *m/z* ($M+H^+$) = 453.1035 (Calculated for $C_{19}H_{23}N_3O_6S_2$ = 453.1028). Solubility (PBS, pH 7.4, 23°C) = 29 ug/mL. Stability profile over 48 hrs (PBS, pH 7.4, 23°C) is shown below in Figure 2.

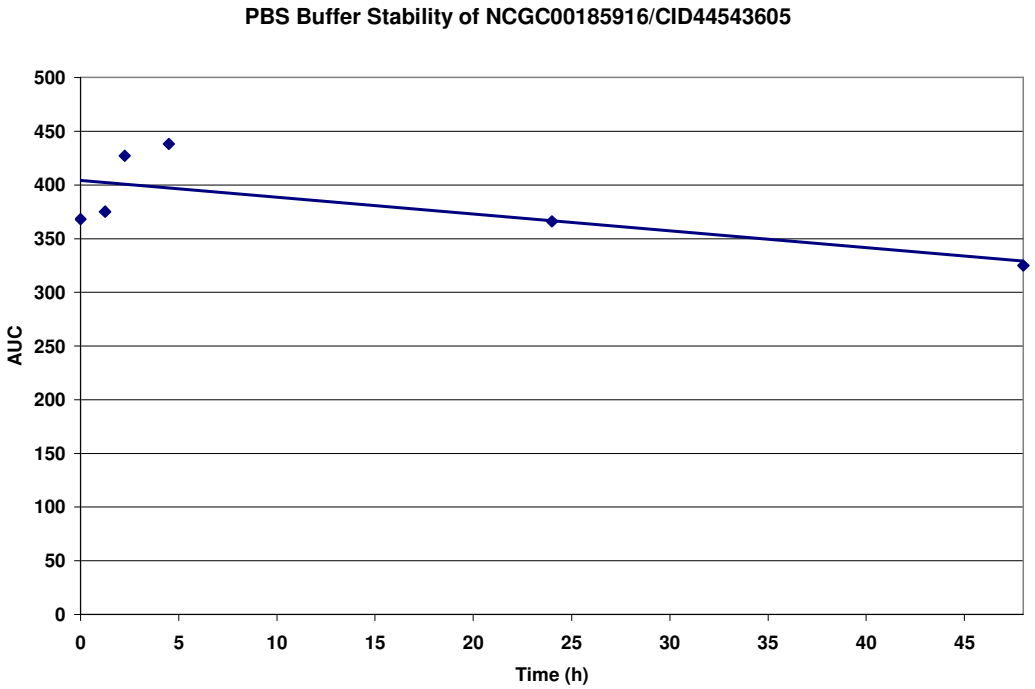

Figure 2. Stability of NCGC00185916/CID44543605/ML203 in PBS buffer (pH 7.4, 23°C) plotted as AUC vs. time for a 48 hr period, using LCMS Method 1 described in Section 2. No significant instability was observed, and >90% of compound remained at 48 hours.

Probe	NCGC00185916	MLS003178529
Analog	NCGC00182833	MLS003178530
Analog	NCGC00181061	MLS003178531
Analog	NCGC00182829	MLS003178532
Analog	NCGC00185923	MLS003178533
Analog	NCGC00168687	MLS003178534

Chemotype #2

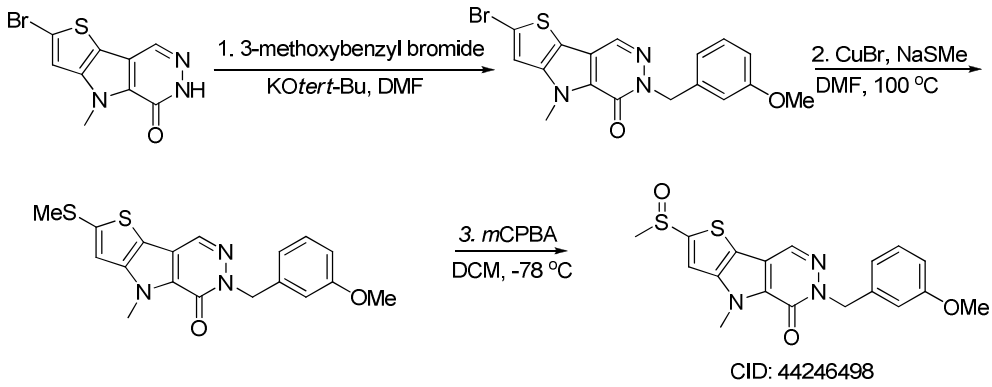

NCGC00186527/CID:44246498/ML202 ^{1}H NMR (400 MHz, $CDCl_3$) δ 8.27 (s, 1H), 7.56 (s, 1H), 7.23 (d, 1H, *J*= 7.6 Hz), 7.00 (dd, 1H, *J*= 7.6, 0.4 Hz), 6.98-6.96 (m, 1H), 6.83-6.79 (m, 1H), 5.42 (s, 2H), 4.33 (s, 3H), 3.78 (s, 3H), 3.00 (s, 3H); LC/MS: Method 1, retention time, 4.962 min; Method 2, retention time, 3.065; HRMS: *m/z* ($M+H^+$) = 388.0790 (Calculated for $C_{18}H_{18}N_3O_3S_2$ = 388.0790). Solubility (PBS, pH 7.4, 23°C) = 37.4 µg/ml. Stability profile over 48 hrs (PBS, pH 7.4, 23°C) is shown below in Figure 3.

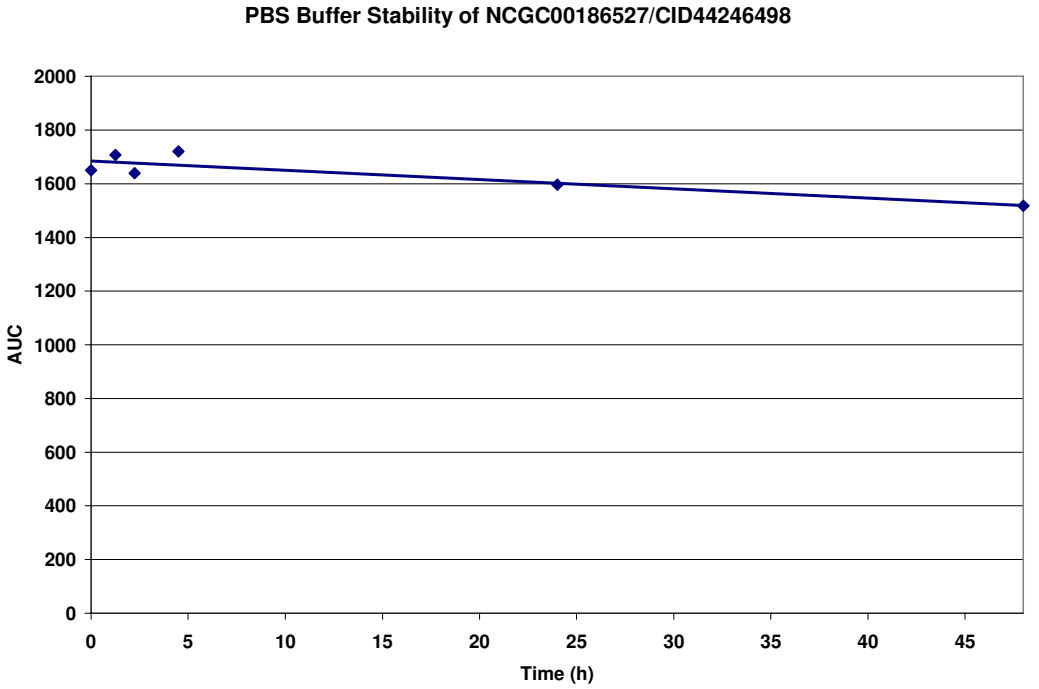

Figure 3. Stability of NCGC00186527/CID44246498/ML202 in PBS buffer (pH 7.4, 23°C) plotted as AUC vs. time for a 48 hr period using LCMS Method 1 described in Section 2. No instability was observed, and 100% of compound remained at 48 hours.

Probe	NCGC00186527	MLS003178535
Analog	NCGC00182625	MLS003178536
Analog	NCGC00182627	MLS003178537
Analog	NCGC00182628	MLS003178538
Analog	NCGC00182629	MLS003178539
Analog	NCGC00186528	MLS003178540

Chemotype #3

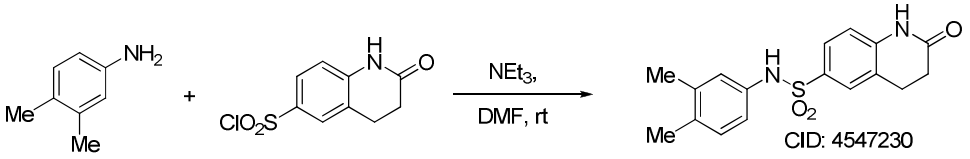

NCGC00185939/CID:4547230/ML170 ^{1}H NMR (400 MHz, DMSO-*d*6) δ ppm: 10.40 (s, 1 H), 9.91 (br. s., 1 H), 7.56 (s, 1 H), 7.51 (dd, *J*=8.41, 1.96 Hz, 1 H), 6.95 (d, *J* =8.22 Hz, 1 H), 6.90 (d, *J*=8.22 Hz, 1 H), 6.86 (s, 1 H), 6.81 (dd, *J*=8.02, 1.96 Hz, 1 H), 2.90 (t, *J*=7.53 Hz, 2 H), 2.46 (t, *J*=7.63 Hz, 2 H), 2.10 (s, 3H), 2.08 (s, 3H). LC/MS: Method 1, retention time: 5.744 min; Method 2, retention time 3.915 min; HRMS: *m/z* (M+) = 330.1032 (Calculated for $C_{17}H_{18}N_2O_3S$ = 330.1038). Solubility (PBS, pH 7.4, 23°C) = >66.7µg/ml. Stability profile over 48 hrs (PBS, pH 7.4, 23°C) is shown below in Figure 4.

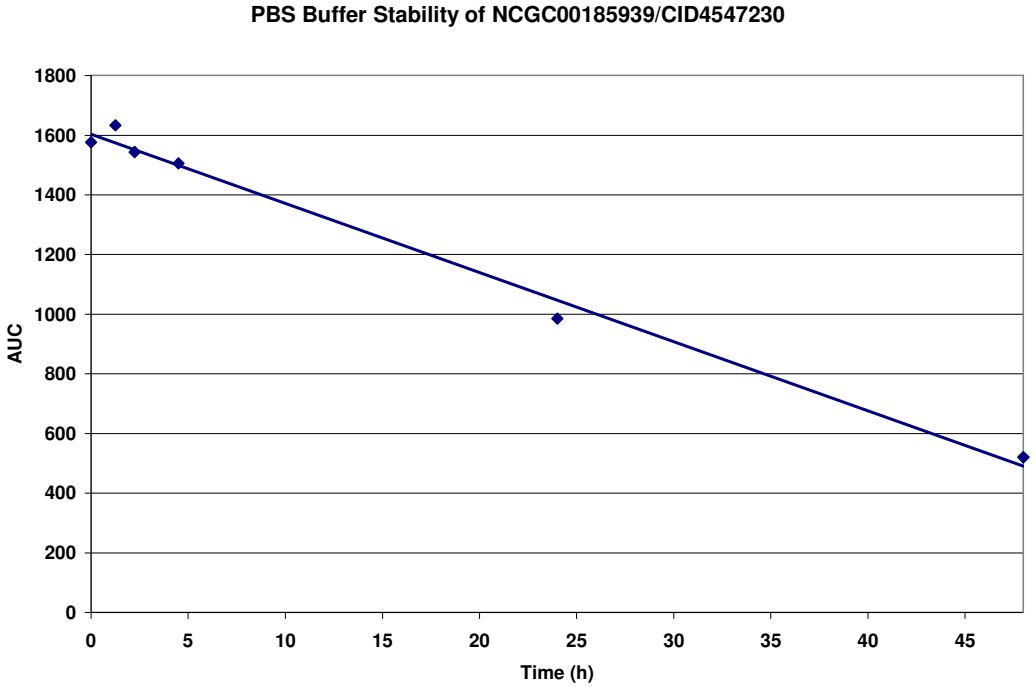

Figure 4. Stability of NCGC00185939/CID4547230/ML170 in PBS buffer (pH 7.4, 23°C) plotted as AUC vs. time for a 48 hr period using LCMS Method 1 described in Section 2. AUC decreased linearly with time, but no side products were detected via LCMS. ~30% of the compound remained at 48 hours.

Probe	NCGC00185939	MLS000673795
Analog	NCGC00187734	MLS003178541
Analog	NCGC00187735	MLS003178542
Analog	NCGC00186542	MLS003178543
Analog	NCGC00186553	MLS003178544
Analog	NCGC00188488	MLS003178545

2.3 Probe Preparations

Synthesis of CID: 44543605/ML203

Step 1. tert-butyl 1,4-diazepane-1-carboxylate (0.75g, 3.74mmol, 1equiv.) was dissolved in dichloromethane (7ml) and cooled in an ice bath under nitrogen atmosphere. Triethylamine (1.04ml, 7.49mmol, 2.0equiv.) was added, followed by portionwise addition of 2,3-dihydrobenzo[b][1,4]dioxine-6-sulfonyl chloride (1.01g, 4.31mmol, 1.15equiv.). The reaction was stirred in the ice bath for one hour, and then quenched with saturated aqueous ammonium chloride (~10ml). The organic layer was washed

twice with saturated ammonium chloride, once with brine, dried over sodium sulfate and concentrated *in vacuo;* it was then purified on silica gel chromatography using a 95/5 – 5/95, hexane/EtOAc (v/v) gradient to give tert-butyl 4-(2,3-dihydrobenzo[b][1,4]dioxin-6-ylsulfonyl)-1,4-diazepane-1-carboxylate as a white powder (1.34 g, 89% yield).

Step 2. tert-butyl 4-(2,3-dihydrobenzo[b][1,4]dioxin-6-ylsulfonyl)-1,4-diazepane-1-carboxylate (1.2g, 3.01mmol, 1equiv.) was dissolved in dichloromethane (5 ml), cooled in an ice bath and TFA (3.48ml, 45.2mmol, 15equiv.) was then added. The reaction was stirred at 0°C for 6 hours, then concentrated *in vacuo* to yield the TFA salt of 1-(2,3-dihydrobenzo[b][1,4]dioxin-6-ylsulfonyl)piperazine, which was carried onto the next step without purification.

Step 3. The TFA salt of 1-(2,3-dihydrobenzo[b][1,4]dioxin-6-ylsulfonyl)-1,4-diazepane (0.50 g, 1.21 mmol, 1 equiv.) was dissolved in dichloromethane (3mk) and cooled in an ice bath. Triethylamine (500µl, 3.64mmol, 3equiv.) was added followed by portionwise addition of 3-acetamidobenzene-1-sulfonyl chloride (0.34g, 1.46mmol, 1.2equiv.). The reaction was allowed to warm to room temperature, and after 1 hour, the reaction was quenched with saturated aqueous ammonium chloride (~3ml). The organic layer was washed twice with saturated ammonium chloride, once with brine, dried over sodium sulfate, concentrated *in vacuo* and then purified on silica gel chromatography using a 99/1 – 9/1, DCM/MeOH (v/v) gradient to give N-(3-(4-(2,3-dihydrobenzo[b][1,4]dioxin-6-ylsulfonyl)-1,4-diazepan-1-ylsulfonyl)phenyl)acetamide as a white powder (0.47 g, 78% yield).

Step 4. In a microwave vial, N-(3-(4-(2,3-dihydrobenzo[b][1,4]dioxin-6-ylsulfonyl)-1,4-diazepan-1-ylsulfonyl)phenyl)acetamide (0.40g, 0.81mmol, 1equiv.) was suspended in ethanol (2ml) and an aqueous solution of 4N HCl (0.4ml, 1.61mmol, 2equiv) was added. The suspension was heated to 80°C for 1 hour in a microwave. After cooling to room temperature, the solvents were removed *in vacuo* and the powder was dissolved in DMSO and purified by reverse phase chromatography to give 3-(4-(2,3-dihydrobenzo[b][1,4]dioxin-6-ylsulfonyl)-1,4-diazepan-1-ylsulfonyl)aniline (NCGC00185916/CID:44543605) as a TFA salt (0.41 g, 89% yield).

Synthesis of CID: 44246498/ML202

Step 1: Potassium *tert*-butoxide (1.15g, 10.24mmol) and 3-methoxybenzylbromide (2.73g, 13.66mmol) were added to a solution of 2-bromo-4-methyl-4H-thieno[3,2-b]pyrrole[3,2-d]pyridazinone (2.00g, 6.83mmol) in DMF (50ml). The mixture was stirred for 5 h at room temperature. H_2O (100 ml) and EtOAc (200 ml) were added to the mixture, and the organic layer was separated. The aqueous layer was further extracted with EtOAc (2x 100ml) and the combined organic layers were washed with brine, dried

over sodium sulfate. After the removal of organic solvent, the residue was purified by column chromatography (EtOAc/hexane: 1/2) to give 2-bromo-4-methyl-6-[(3-methoxyphenyl)-methyl]-4H-thieno[3,2-b]pyrrole[3,2-d]pyridazinone (2.26 g, 82%) as a white solid.

Step 2: CuBr (0.72mg, 5.00mmol) and NaSMe (706mg, 15.00mmol) were added to a solution of 2-bromo-4-methyl-6-[(3-methoxyphenyl)methyl]-4H-thieno[3,2-b]pyrrole[3,2-d]pyridazinone (2.06g, 5.00mmol) in DMF (25ml), and the reaction flask was purged with nitrogen and sealed. The mixture was heated at 10^{o}C (oil bath) for 16 h. After cooling to room temperature, H_2O (50ml) was added to the mixture and the precipitate was filtered through a pad of Celite. The filtrate was extracted with EtOAc (3x 50ml). The combined organic layers were washed with brine, dried over sodium sulfate. After the removal of organic solvent, the crude product was purified by column chromatography (EtOAc/hexane: 1/1) to give 2-methylthio-4-methyl-6-[(3-methoxy-phenyl)methyl]-4H-thieno[3,2-b]pyrrole[3,2-d]pyridazinone (1.67g, 90%) as a white solid.

Step 3: A solution of 2-methylthio-4-methyl-6-[(3-methoxyphenyl)methyl]-4H-thieno[3,2-b]pyrrole[3,2-d]pyridazinone (1.20g, 3.23mmol) in DCM (20 ml) was cooled to -78^{o}C. To this cold solution, *m*CPBA solution (0.67g, 3.88mmol in 10ml DCM) was added dropwise (the addition was completed in 15 min). The mixture was further stirred at -78^{o}C for 30 min and quenched with aqueous saturated $NaHCO_3$ solution (*ca*. 5ml). After warming to room temperature, the mixture was washed with aqueous saturated $NaHCO_3$ solution (20ml), and the organic layer was separated. The aqueous layer was further extracted with DCM (2x 20ml) and the combined organic layers were washed with brine, dried over sodium sulfate. After the removal of organic solvent, the crude product was purified by column chromatography (MeOH/DCM: 1/20) to give 2-methylsulfinyl-4-methyl-6-[(3-methoxyphenyl)methyl]-4H-thieno[3,2-b]pyrrole[3,2-d]-pyridazinone (NCGC00186527/CID:44246498) (1.06 g, 85%) as a white solid.

Synthesis of CID: 4547230/ML170

2-oxo-1,2,3,4-tetrahydroquinoline-6-sulfonyl chloride (0.20g, 0.81mmol, 1equiv.) was dissolved in DMF (2ml) and 3,4-dimethylaniline (0.118g, 0.98mmol, 1.2equiv.) was added, followed by the dropwise addition of DIPEA (0.213ml, 1.22mmol, 1.5equiv.). The reaction was stirred at RT for 1 h, then purified by directly injecting to a Waters® reverse phase purification system to give N-(3,4-dimethylphenyl)-2-oxo-1,2,3,4-tetrahydroquinoline-6-sulfonamide (NCGC00185939/CID:4547230) as a TFA salt (0.26 g, 72%).

3 Results

Please see subsections for detailed results.

3.1 Summary of Screening Results

Primary assay summary

The assay showed excellent performance (the signal-to-background ratio was 6.9 +/- 1.6, the average Z' screening factor associated with each plate was 0.78 +/- 0.07, and the CV was 10.0 +/- 2.6, indicating a robust performance of the screen). A total of 125 actives were selected for confirmation (AID:1751).

Activity	Distribution	Curve Classification						
		1a	1b	2a	2b	3	4	5
Activation	No. Cmpds.	**134**	**318**	**325**	**1541**	2094		
	% library	0.05	0.11	0.11	0.55	0.74	276309	1
Inhibition	No. Cmpds.	**4**	**25**	**31**	**582**	983	97.73%	0.00%
	% library	0.00	0.01	0.01	0.21	0.35		

Table 2. Concentration-Response Curve Class Distribution from Primary Screen

Identification of lead

The results of this screening effort are detailed in Table 2. Small molecule activators of PKM2 were more prevalent than inhibitors, occurring at 0.27% for high confidence 1a, 1b and 2c concentration-response curves (CRCs; class 1 curves display two asymptotes, an inflection point, and $r^2 \geq 0.9$; subclasses 1a and 1b are differentiated by full (>80%) vs. partial (≤ 80%) response, respectively, while class 2a curves display a single left-hand asymptote and inflection point and full (>80%) response)[9]. Note: subsequent analysis has shown that apparent inhibitors are primarily inhibitors of the Kinase-Glo detection reagent. A cheminformatics analysis of the qHTS data included chemotype clustering, singleton identification, analysis of orthogonal activities, and structural considerations, which included physical properties and anticipated optimization potential. Potency range and maximum response were additionally considered. Ultimately, this analysis led us to focus on the substituted *N*,*N*'-diarylsulfonamide NCGC00030335 (CID_650361, SID_847943, detailed in reference 10), the substituted heterocycle NCGC00031955 (CID_654376, SID_851783, detailed in reference 11), and the substituted tetrahydroquinoline-6-sulfonamide NCGC00185939-01 (CID_4547230, SID_85176568).

3.2 Dose Response Curves for Probes

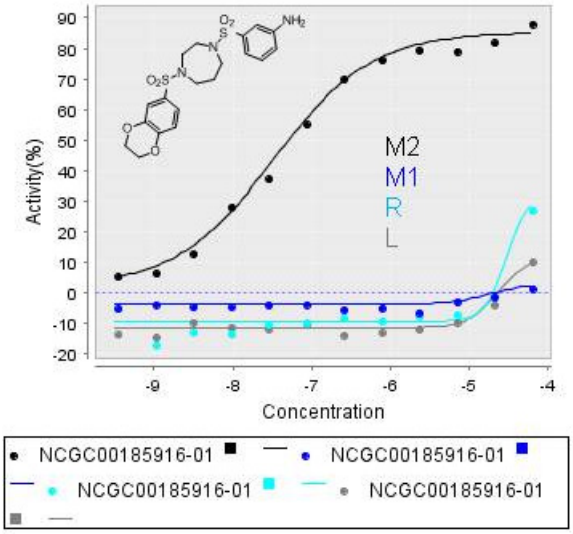

Figure 5. Dose response curves for NCGC00185916/CID_44543605/ML203 against the four hPyk isozymes.

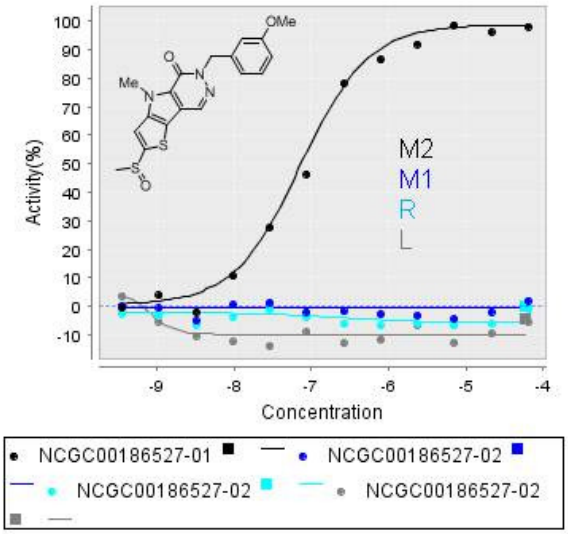

Figure 6. Dose response curves for NCGC00186527/ CID_44246498/ML202 against the four hPyk isozymes.

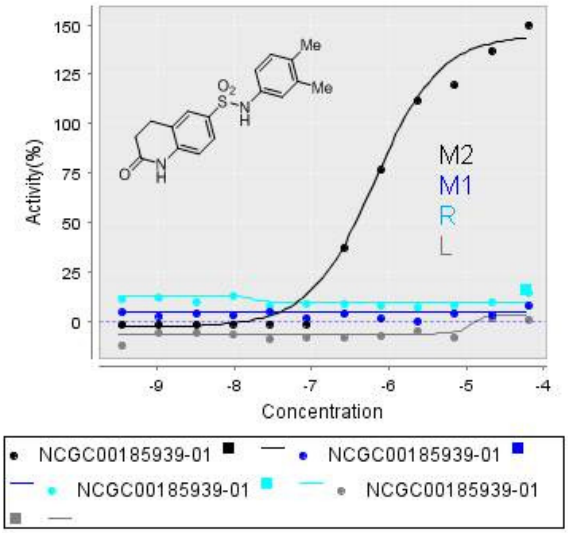

Figure 7. Dose response curves for NCGC00185939/ CID_4547230/ML170 against the four hPyk isozymes.

3.3 Scaffold/Moiety Chemical Liabilities

NCGC00185916/CID:44543605 contains an unsubstituted aniline functionality that may be liable to *in vivo* metabolism. NCGC00186527/CID:44246498 contains a thiophene ring which may be liable to *in vivo* metabolism. NCGC00185939/CID:4547230 does not contain any obvious chemical liabilities.

3.4 SAR Tables

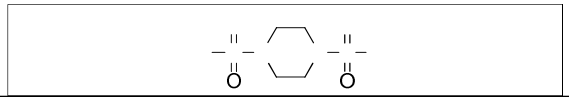

entry	Internal ID[a]	CID	SID	n	Ar_1	Ar_2	*hPyk, M2* AC_{50} *(mM)*[b]
1	NCGC00030335	650361	847943	1	4-methoxybenzene	6-(2,3-dihydrobenzo[*b*][1,4]dioxine)	0.562
2	NCGC00181063	25243716	57646218	1	2,4,5-trifluorobenzene	6-(2,3-dihydrobenzo[*b*][1,4]dioxine)	0.708
3	NCGC00181075	46925859	99430930	1	2-trifluoromethoxybenzene	6-(2,3-dihydrobenzo[*b*][1,4]dioxine)	1.00
4	NCGC00182418	44543577	87225662	1	4-bromo-2,5-difluorobenzene	6-(2,3-dihydrobenzo[*b*][1,4]dioxine)	4.47
5	NCGC00182431	44543587	87225672	1	4-carboxlic acid-2,5-difluorobenzene	6-(2,3-dihydrobenzo[*b*][1,4]dioxine)	15.8
6	NCGC00182435	44543590	87225676	1	4-(carboxymethyl)-2,5-difluorobenzene	6-(2,3-dihydrobenzo[*b*][1,4]dioxine)	17.8
7	NCGC00182423	25243745	57646260	1	4-(*n*Propyl)-2,5-difluorobenzene	6-(2,3-dihydrobenzo[*b*][1,4]dioxine)	31.6
8	NCGC00182430	44543586	87225671	1	4-Me-carboxylate-2,5-difluorobenzene	6-(2,3-dihydrobenzo[*b*][1,4]dioxine)	0.224
9	NCGC00182834	16272009	99430931	1	3-carboxylic acid benzene	6-(2,3-dihydrobenzo[*b*][1,4]dioxine)	0.355
10	NCGC00168675	25243709	57646209	1	3-methoxybenzene	6-(2,3-dihydrobenzo[*b*][1,4]dioxine)	0.447
11	NCGC00182822	25243772	57646289	1	2,6-difluorophen-3-ol	6-(2,3-dihydrobenzo[*b*][1,4]dioxine)	0.562
12	NCGC00182825	25243773	57646290	1	2,6-difluoro-4-methoxybenzene	6-(2,3-dihydrobenzo[*b*][1,4]dioxine)	1.00
13	NCGC00168687	25243713	57646214	1	benzene	6-(2,3-dihydrobenzo[*b*][1,4]dioxine)	1.21
14	NCGC00182833	25243777	57646295	1	3-trifluoromethyl	6-(2,3-dihydrobenzo[*b*][1,4]dioxine)	1.26
15	NCGC00181059	25243715	57646216	1	2,4-difluorobenzene	6-(2,3-dihydrobenzo[*b*][1,4]dioxine)	1.58
16	NCGC00181061	25210493	57646217	1	2,6-difluorobenzene	6-(2,3-dihydrobenzo[*b*][1,4]dioxine)	0.065
17	NCGC00182829	25243775	57646292	2	2,6-difluorobenzene	6-(2,3-dihydrobenzo[*b*][1,4]dioxine)	0.866
18	NCGC00185917	44543606	87225695	1	3-aniline	2,6-difluoro-4-methoxybenzene	0.023
19	NCGC00185919	44543608	87225697	1	3-aniline	6-(2,3-dihydrobenzo[*b*][1,4]dioxine)	0.041
20	NCGC00185921	44543609	87225699	1	3-aniline	2,6-difluorobenzene	0.092
21	NCGC00185923	44543611	87225701	2	3-aniline	2,6-difluoro-4-methoxybenzene	0.206
22	NCGC00185916	44543605	87225694	2	3-aniline	6-(2,3-dihydrobenzo[*b*][1,4]dioxine)	0.033

[a]All compounds synthesized at NCGC
[b]AC50 values were determined utilizing the luminescent pyruvate kinase-luciferase coupled assay

Table 3. SAR of selected *N,N*-bisarylsulfonamides

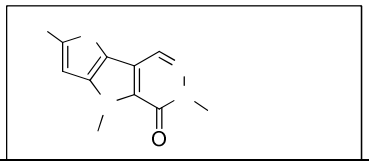

Entry	Internal ID[a]	SID	CID	R'	R''	*hPykM2 AC50 (μM)[b]*
1	NCGC00182626	57646264	25243749	Methyl	2,3-difluoro-4-methylbenzyl	0.057
2	NCGC00182628	57646265	25243750	Methyl	2,4-difluorobenzyl	0.025
3	NCGC00182629	99376599	46912194	Methyl	2,5-difluorobenzyl	0.631
4	NCGC00182637	57646268	25243753	Methyl	2,6-difluorobenzyl	0.025
5	NCGC00182642	57646269	25243754	Methyl	2-chloro-6-fluorobenzyl	0.040
6	NCGC00182645	57646270	25243755	Methyl	2,3-difluorobenzyl	0.113
7	NCGC00182646	57646271	25243756	Methyl	2,3,4-trifluorobenzyl	0.713
8	NCGC00182631	99376600	46912195	Methyl	2,4,5-trifluorobenzyl	0.355
9	NCGC00182623	99376596	46912191	Methyl	3-chloro-2-fluorobenzyl	0.447
10	NCGC00182625	99376597	46912192	Methyl	6-chloro-2-fluoro-3-methylbenzyl	1.120
11	NCGC00182784	99431075	16670259	Methyl	3-methoxybenzyl	0.282
12	NCGC00182782	99431074	46925942	Methyl	3-trifluoromethylbenzyl	1.780
13	NCGC00182780	99431073	46925941	Methyl	3-methylbenzyl	0.631
14	NCGC00182774	57646277	25243761	Methyl	3-chlorobenzyl	0.794
15	NCGC00031955	851783	654376	Methyl	2-fluorobenzyl	0.130
16	NCGC00182412	57646256	25243741	S(O)Me	2-fluorobenzyl	0.025
17	NCGC00186527	85267884	44246498	S(O)Me	3-methoxybenzyl	0.073
18	NCGC00186528	85267885	44246499	S(O)Me	3-(methyl)aniline	0.092
19	NCGC00187749	87225720	44543627	S(O)Me	3-(methyl)phenol	0.041

[a]All compounds synthesized at NCGC
[b]AC50 values were determined utilizing the luminescent pyruvate kinase-luciferase coupled assay.

Table 4. SAR of selected thieno[3,2-b]pyrrole[3,2-d]pyridazinones

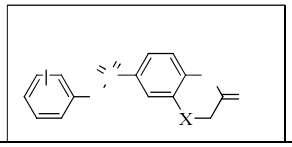

entry	Internal ID[a]	CID	SID	R_1	R_2	X	*hPykM2 AC_{50} (μM)[b]*
1	NCGC00185939	4547230	85176568	H	3,4-dimethyl	CH_2	0.65
2	NCGC00186544	3647906	87915628	H	3-chloro	CH_2	0.65
3	NCGC00186538	7066682	87915622	H	meta-tolyl	CH_2	1.20
4	NCGC00186537	3648364	87915621	H	ortho-tolyl	CH_2	3.90
5	NCGC00186539	3656150	87915623	H	para-tolyl	CH_2	4.10
6	NCGC00187757	44623906	87550905	F	3,4-dimethyl	CH_2	0.92
7	NCGC00187734	22548477	87550883	Cl	3,4-dimethyl	O	0.58
8	NCGC00187735	38888103	87550884	Br	3,4-dimethyl	O	18
9	NCGC00187741	22548371	87550890	Me	3,4-dimethyl	O	1.2

[a]All compounds synthesized at NCGC
[b]AC50 values were determined utilizing the luminescent pyruvate kinase-luciferase coupled assay.

Table 5. SAR of selected tetrahydroquinoline-sulfonamides

3.5 Cellular Activity

In collaboration with researchers at Harvard, MIT and Agios Pharmaceuticals, we are conducting numerous cell based experiments examining the correction of the Warburg effect and the antiproliferative nature of these compounds (both *in vitro* and *in vivo*). These studies detail both the mechanism of these agents with cells and explore the compounds' ability to alter oxygen uptake and lactic acid production. These studies are at various stages of completion (publication pending).

3.6 Profiling Assays

There are no profiling assays available for all 3 probes.

4 Discussion

Investigation of the SAR around the *N,N*-bisarylsulfonamides indicated that while holding the 6-(2,3-dihydrobenzo[b][1,4]dioxine) constant, substitution at the 4-position of the other aryl ring generally resulted in a large drop in potencies (i.e. entries 5-7). Smaller changes around the aryl ring generally did not affect potencies greatly. With the goal of improving solubility and potentially gaining potency and/or efficacy by forming hydrogen bonds with the protein, both 3-carboxylic acid and 3-anilino functionalities were tested, and the aniline derivative proved to be ~10 fold more potent (compare entries 9 and 19). The piperazine ring was then modified to the homopiperazine analog, which resulted in a similarly potent analog, but had much improved aqueous solubility (4.1 µg/ml for NCGC00185919 vs 29.0 µg/ml for NCGC00185916). This potency and solubility profile led us to declare NCGC00185915/CID_44543605 as the probe for this series.

Examination of the SAR around two areas of the thieno[3,2-b]pyrrole[3,2-d]pyridazinones was investigated. First, various substituted benzyl groups were screened, and resulted in considerable tolerance at all positions. Most of the compounds had potencies < 1.0µM, with the exception of 6-chloro-2-fluoro-3-methylbenzyl and 3-trifluoromethylbenzyl groups. The methyl group on the thiophene ring was modified to a methyl sulfoxide functionality, which saw a large improvement in potency, but only a modest improvement of solubility (compare entries 15 and 16). Replacement of the 2-fluorobenzyl group with the 3-methoxybenzyl group (entry 17) saw a slight drop in potency, but a large improvement in solubility (from 4.4 µg/ml to 37.4 µg/ml). This potency and solubility profile led us to declare NCGC00186527/CID_ 44246498 as the probe for this series.

The tetrahydroquinoline-sulfonamide series was diversified at three different points. First, R_2 was varied and it was found that both the 3,4-dimethyl and 3-chloro substitution had similar potencies (entries 1 and 2). Interestingly, the 3-methyl- and 4-methyl-analogs saw a loss in activity (entries 3 and 4). Substitution at the R_1 position was tolerant to fluorine with a slight loss of potency. Substitution of oxygen in the tetrahydroquinoline ring with accompanying chlorine substitution resulted in a slight improvement in potency, while bromine or methyl substitution saw a significant loss in activity (entries 7 – 9). While NCGC00187734 showed a slight improvement in potency, the aqueous solubility was considerably lower (1.4 µg/ml compared to >66.7 µg/ml), which led us to nominate NCGC00185939/CID4547230 as the probe.

4.1 Comparison to existing art and how the new probe is an improvement

Prior to our discovery of these hPykM2 activators, there were no reported small molecule modulators of this enzyme.

4.2 Mechanism of Action Studies

We examined the mode of action for these probes versus hPykM2, through analysis of the steady-state kinetics of PEP and ADP by the hPykM2. Fructose-1,6-bisphosphate is known to allosterically activate hPykM2 through induction of an enzyme state with a high affinity for PEP. In the absence of any of these activators, hPyk shows low affinity for PEP (K_M ~ 1.5mM). In the presence of NCGC00031955 (CID_654376, SID_851783) or NCGC00030335 (CID_650361, SID_847943) or FBP, the K_M for PEP decreased 10-fold to 0.13±0.04 mM or 0.1±0.02 mM for the two activators, respectively, with lesser effects on V_{max} (values of 245 pmols/min with or without FBP and 255 pmols/min with NCGC00031955: CID_654376, SID_851783). In contrast, variation of the concentration of ADP in the presence and absence of activators shows that the steady-state kinetics are not significantly affected (K_M for ADP = 0.1mM in either condition). Thus, NCGC00031955 (CID_654376, SID_851783) and NCGC00030335 (CID_650361, SID_847943) activate hPykM2by increasing the enzyme's affinity for PEP and have little effect on ADP kinetics. This is similar to what we observed for FBP, which agrees with previous reports demonstrating increased affinity for PEP as the reason for activation of hPykM2 by FBP. We are currently examining the three probes to determine if they all have the similar mechanism of action.

In collaboration with researchers at the Structural Genomics Consortium, we have pursued the X-ray structure of NCGC00186527 (CID_44246498) and NCGC00185916 (CID_44543605) bound to hPykM2; we noted that they induce tetramization of the enzyme via binding to an allosteric site spanning the dimer interface (publication pending). We are currently examining NCGC00185939 (CID_4547230, SID_85176568) to determine if this chemotype binds in a similar manner. In collaboration with researchers at Harvard, MIT and Agios Pharmaceuticals, we have conducted numerous cell based experiments examining the correction of the Warburg effect and the antiproliferative nature of these compounds (both *in vitro* and *in vivo*). These studies both detail the mechanism of these agents with cells and explore the compounds' ability to alter oxygen uptake and lactic acid production. These studies are at various stages of completion (publication pending).

4.3 Planned Future Studies

The discovery and optimization of these probes was primarily guided by potency and selectivity over the other human isoforms. These goals were successfully accomplished, as all three chemotypes activate the M2 isoform with low nanomolar activity, but do not activate nor inhibit human isoforms L, R or M1. The aim is to develop these probes into pharmacological agents able to halt tumor growth *in vivo* using mouse cancer models. Extended characterization and optimization of these molecules to engender proper PK-ADME properties to accompany the selectivity and potency is necessary. It is envisioned that all three

chemotypes can be carried through this strategy concurrently to identify lead(s) that are appropriate for *in vivo* studies (Figure 8).

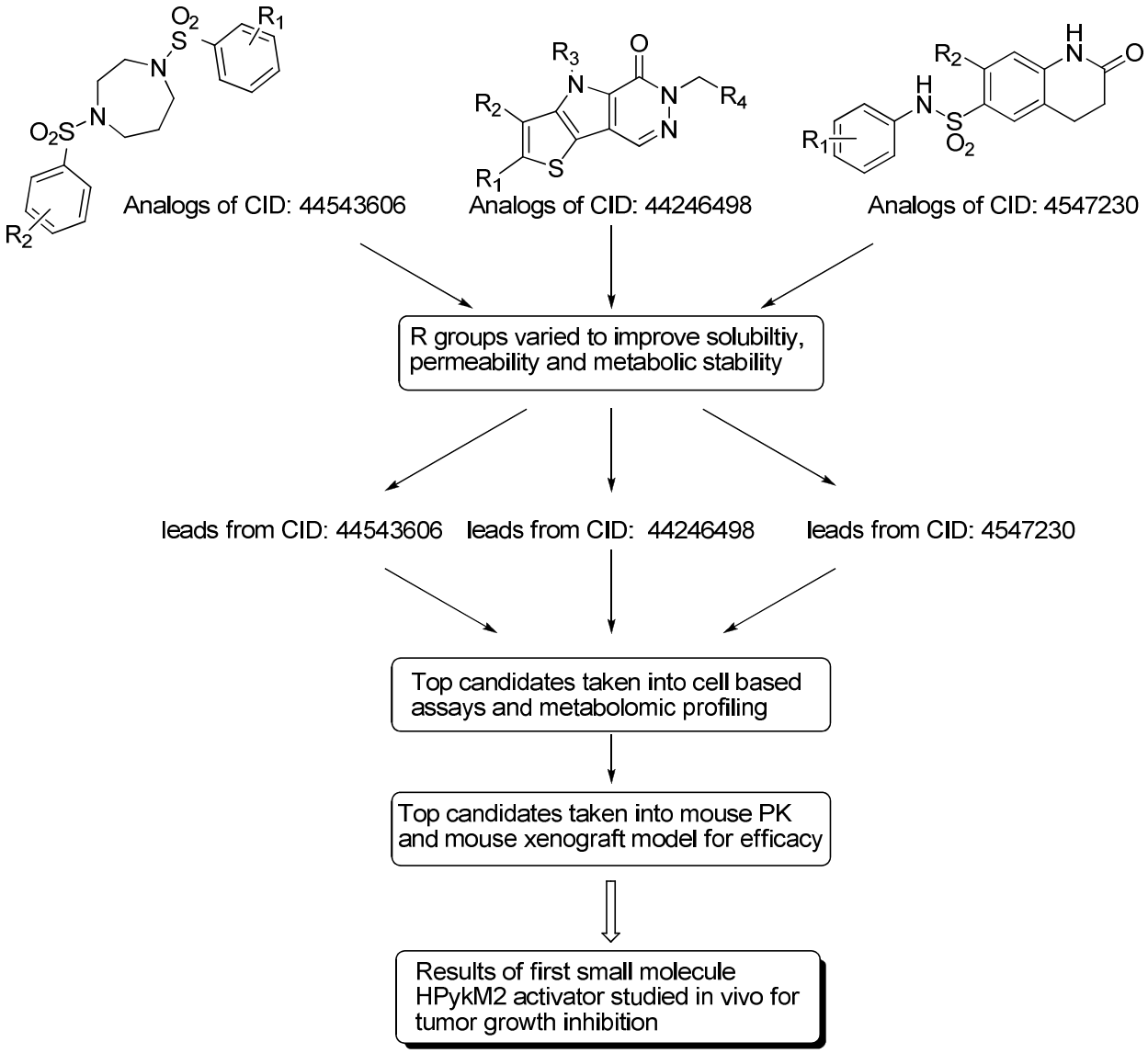

Figure 8. Critical Workflow to Lead to *in vivo* studies of HPykM2 activators.

Biology Research Plan: All lead compounds emerging from the established *in vitro* assays will be characterized in a cancer cell line assay that will confirm if compounds can enter cells and stabilize the pykM2 tetramer (Vander Heiden lab, unpublished results). Lactate production and oxygen consumption can be used to confirm cell-based activity using M1 and M2 expressing cells treated with compound[6]. A more detailed metabolic characterization using isotopically labeled glucose and mass spectrometry will also be carried out to understand how lead compounds influence cell

metabolism (Vander Heiden lab). Compounds showing efficacy in the cell-based assays will be assessed in mouse PK studies to determine distribution and availability, and inform on dosing. Compounds emerging with desirable PK properties will then be evaluated in mouse cancer models. Initially, these models will evaluate the ability of these molecules to halt tumor progression of H1299 xenograft models where pykM1 expression is known to inhibit growth[6]. Later, the studies will be expanded to engineered mouse models of human cancer.

Probe properties

Properties computed from Structure:

Calculated Property	Probe Identity		
	Chemotype 1	Chemotype 2	Chemotype 3
	CID_44543605 (MLS003178529)	CID_44246498 (MLS003178535)	CID_4547230 (MLS000673795)
Molecular Weight [g/mol]	453.53242	387.47588	330.40142
Molecular Formula	C19H23N3O6S2	C18H17N3O3S2	C17H18N2O3S
XLogP3-AA	1.1	2	2.3
H-Bond Donor	1	0	2
H-Bond Acceptor	9	4	4
Rotatable Bond Count	4	4	3
Tautomer Count	0	0	3
Exact Mass	453.102827	387.071133	330.103813
MonoIsotopic Mass	453.102827	387.071133	330.103813
Topological Polar Surface Area	136	111	83.6
Heavy Atom Count	30	26	23
Formal Charge	0	0	0
Isotope Atom Count	0	0	0
Defined Atom StereoCenter Count	0	0	0
Undefined Atom StereoCenter Count	0	1	0
Defined Bond StereoCenter Count	0	0	0
Undefined Bond StereoCenter Count	0	0	0
Covalently-Bonded Unit Count	1	1	1
Complexity	794	617	543

5 References

1. Vander Heiden, M. G.; Cantley, L. C.; Thompson, C. B. Understanding the Warburg Effect: The Metabolic Requirements of Cell Proliferation. *Science* **2009**, *324*, 1029-1033.
2. Warburg, O. On the origin of cancer cells. *Science* **1956**, *123*, 309-314.
3. Warburg, O. On respiratory impairment in cancer cells. *Science* **1956**, *124*, 269-270.
4. Mazurek, S.; Boschek, C. B.; Hugo, F.; Eigenbrodt, E. Pyruvate kinase type M2 and its role in tumor growth and spreading. *Semin. Cancer Biol.* **2005**, *15*, 300-308.
5. Takenaka, M.; Noguchi, T.; Sadahiro, S.; Hirai, H.; Yamada, K.; Matsuda, T.; Imai, E.; Tanaka, T. Isolation and characterization of the human pyruvate kinase M gene. *Eur. J. Biochem.* **1991**, *198*, 101-106.
6. Christofk, H. R.; Vander Heiden, M. G.; Harris, M. H.; Ramanathan, A.; Gerszten, R. E.; Wei, R.; Fleming M. D.; Schreiber, S. L.; Cantley, L. C. The M2 splice isoform of pyruvate kinase is important for cancer metabolism and tumor growth. *Nature* **2008**, *452*, 230-233.
7. Christofk, H. R.; Vander Heiden, M. G.; Wu, N.; Asara, J. M.; Cantley, L. C. Pyruvate kinase M2 is a phosphotyrosine binding protein. *Nature* **2008**, *452*, 181-186.
8. Singh, P.; Harden, B. J.; Lillywhite, B. J.; Broad, P. M. Identification of kinase inhibitors by an ATP depletion method. *Assay Drug Dev Technol* **2004**, *2*, 161-9
9. Inglese, J.; Auld, D. S.; Jadhav, A.; Johnson, R. L.; Simeonov, A.; Yasgar, A.; Zheng, W.; Austin, C. P. Quantitative high-throughput screening: A titration-based approach that efficiently identifies biological activities in large chemical libraries. *Proc Natl Acad Sci U.S.A.* **2006**, *103*, 11473-8.
10. Boxer, M. B.; Jiang, J.-K.; Vander Heiden, M. G.; Shen, M.; Skoumbourdis, A. P.; Southall, N.; Veith, H.; Leister, W.; Austin, C. P.; Park, H. W.; Inglese, J.; Cantley, L. C.; Auld, D. S.; Thomas, C. J. Evaluation of substituted N,N'-diarylsulfonamides as activators of the tumor cell specific M2 isoform of pyruvate kinase. *J. Med. Chem.* **2010**, *53*, 1048.
11. Jiang, J.-K.; Boxer, M. B.; Vander Heiden, M. G.; Shen, M.; Skoumbourdis, A. P.; Southall, N.; Veith, H.; Leister, W.; Austin, C. P.; Park, H. W.; Inglese, J.; Cantley, L. C.; Auld, D. S.; Thomas, C. J. Evaluation of thieno[3,2-b]pyrrole[3,2-d]pyridazinones as activators of the tumor cell specific M2 isoform of pyruvate kinase. *Bioorg. Med. Chem. Lett.* **2010**, *20*, 3387-3393.